

# An origin of arc structures deeply embedded in dense molecular cloud cores

Tomoaki Matsumoto<sup>1\*</sup>, Toshikazu Onishi<sup>2</sup>, Kazuki Tokuda<sup>2</sup>, and Shu-ichiro Inutsuka<sup>3</sup>

<sup>1</sup>*Faculty of Humanity and Environment, Hosei University, Fujimi, Chiyoda-ku, Tokyo 102-8160, Japan*

<sup>2</sup>*Department of Physical Science, Graduate School of Science, Osaka Prefecture University, 1-1 Gakuen-cho, Naka-ku, Sakai, Osaka 599-8531, Japan*

<sup>3</sup>*Department of Physics, Nagoya University, Chikusa-ku, Nagoya 464-8602, Japan*

1 August 2018

## ABSTRACT

We investigated the formation of arc-like structures in the infalling envelope around protostars, motivated by the recent Atacama Large Millimeter/Submillimeter Array (ALMA) observations of the high-density molecular cloud core, MC27/L1521F. We performed self-gravitational hydrodynamical numerical simulations with an adaptive mesh refinement code. A filamentary cloud with a 0.1 pc width fragments into cloud cores because of perturbations due to weak turbulence. The cloud core undergoes gravitational collapse to form multiple protostars, and gravitational torque from the orbiting protostars produces arc structures extending up to a 1000 AU scale. As well as on a spatial extent, the velocity ranges of the arc structures,  $\sim 0.5 \text{ km s}^{-1}$ , are in agreement with the ALMA observations. We also found that circumstellar disks are often misaligned in triple system. The misalignment is caused by the tidal interaction between the protostars when they undergo close encounters because of a highly eccentric orbit of the tight binary pair.

**Key words:** hydrodynamics – ISM: clouds – ISM: kinematics and dynamics – stars: formation – turbulence.

## 1 INTRODUCTION

It has been thought that multiple stars are formed through fragmentation from a high density portion of a molecular cloud core. The fragmentation occurs deep inside the molecular cloud core and it has not ever been observed directly.

MC27 (Mizuno et al. 1994; Onishi et al. 1999, 2002) or L1521F (Codella et al. 1997) is a dense cloud core in Taurus and observations have suggested that MC27/L1521F is in a very early stage of star formation (Onishi et al. 1999). Recently Tokuda et al. (2014) performed Atacama Large Millimeter/Submillimeter Array (ALMA) observations on dust continuum emission and molecular rotational lines toward MC27/L1521F. One of their new findings is an arc structure with a  $\sim 2000$  AU length at the center of the molecular cloud core, suggesting that the arc structure can be attributed for a dynamical interaction between envelope gas and dense gas condensations. They also suggested that the turbulence promotes fragmentation of cloud cores during the collapse as shown by the numerical simulations of turbulent cloud cores (e.g., Bate et al. 2002; Goodwin et al. 2004). In these numerical simulations, the orbital motion of fragments excite spiral arms in the center of the cloud core. However, these

studies focus mainly on the physical fragmentation process, while the observable features, such as the velocity structure of spiral arms, are still poorly understood.

In this paper, the protostellar collapse of a turbulent core is calculated from a parent filamentary cloud by using adaptive mesh refinement (AMR) simulations. We reproduced arc structures on a scale of about 1000 AU at the central part of the molecular cloud core. Based on these simulations, the formation mechanism of the arc structures is discussed. This paper is organized as follows. In section 2, the models and simulation methods are presented. The results of the simulations are shown in section 3, and they are discussed in section 4.

## 2 MODELS AND METHODS

A filamentary molecular cloud is considered as the initial condition for this study because recent observations have revealed that filaments are basic compositions of molecular clouds (e.g., André et al. 2010; Hacar et al. 2013). The filament is assumed to be infinitely long and in an equilibrium state where thermal pressure supports an isothermal cloud against its self-gravity. The cloud therefore has a density distribution of  $\rho(R) = \rho_0(1 + R^2/R_0^2)^{-2}$ , where  $R$ ,  $\rho_0$  and  $R_0$  are a cylindrical radius, density on the filamentary axis, and

\* E-mail: mats@hosei.ac.jp

a scale height of the filament, respectively (Stodólkiewicz 1963; Ostriker 1964). We set  $R_c = 0.05$  pc, which mimics filaments observed by the Herschel survey (Arzoumanian et al. 2011). The gas temperature was assumed to be  $T = 10$  K at the initial stage and the corresponding sound speed is  $c_s = 0.190$  km s<sup>-1</sup>. The density on the filamentary axis is given by  $\rho_0 = 2c_s^2/(\pi GR_0^2) = 1.45 \times 10^{-19}$  g cm<sup>-3</sup> (the corresponding number density is  $n_0 = 3.79 \times 10^4$  cm<sup>-3</sup>). The barotropic equation of state was assumed to be  $P(\rho) = c_s^2 \rho + \kappa \rho^{7/5}$  with  $\kappa = c_s^2 \rho_{\text{cr}}^{-2/5}$ , where the critical density is set at  $\rho_{\text{cr}} = 10^{-13}$  g cm<sup>-3</sup> (the corresponding number density is  $n_{\text{cr}} = 2.62 \times 10^{10}$  cm<sup>-3</sup>), which was taken from the numerical results of Masunaga, Miyama, & Inutsuka (1998). The magnetic field was ignored for simplicity. The computational domain is a cubic box with side lengths  $L = 4\lambda_{\text{max}} = 1.56$  pc, where  $\lambda_{\text{max}} (= 7.81 R_0)$  is the wavelength of the most unstable perturbation against fragmentation of the filament (Nagasawa 1987). Periodic boundary conditions were imposed.

Turbulence was imposed at the initial stage. The initial velocity field is incompressible with a power spectrum of  $P(k) \propto k^{-4}$ , generated according to Dubinski et al. (1995), where  $k$  is the wavenumber. This power spectrum results in a velocity dispersion of  $\sigma(\lambda) \propto \lambda^{1/2}$ , in agreement with the Larson scaling relations (Larson 1981). The root mean square (rms) Mach number in the computational domain was set at unity. Note that the rms Mach number on a 0.1 pc scale is expected to be  $\sim 0.25$  according to the scaling relations, and the turbulence is therefore subsonic on the filament scale. Such a subsonic turbulence was suggested by the narrow molecular line widths of dense cores in Taurus (Onishi et al. 1998).

The evolution of the filamentary cloud was calculated using three-dimensional AMR code, SFUMATO (Matsumoto 2007). The hydrodynamic scheme was modified to have a third order of accuracy in space and a second order in time. The computational domain is resolved on a base grid of  $l = 0$  with  $256^3$  cells. The maximum grid level was set at  $l = 11$ . The cell width is  $\Delta x_{\text{min}} = 0.613$  AU on the finest grid of  $l = 11$ , compared with  $\Delta x_{\text{max}} = 1.26 \times 10^3$  AU on the base grid of  $l = 0$ . The Jeans condition was employed as a refinement criterion; blocks are refined when the Jeans length is shorter than 8 times the cell width, i.e.,  $\lambda_J < 8\Delta x$ , where  $\lambda_J$  is the Jeans length (c.f., Truelove et al. 1997).

The sink particle is introduced as a sub-grid model of protostars. The detailed implementations of the sink particles are shown in Matsumoto et al. (2015). The critical density for sink particle formation is set at  $\rho_{\text{sink}} = 1 \times 10^{-11}$  g cm<sup>-3</sup> ( $n_{\text{sink}} = 2.62 \times 10^{12}$  cm<sup>-3</sup>), and the sink radius is set at  $r_{\text{sink}} = 4\Delta x_{\text{min}} = 2.45$  AU.

### 3 RESULTS

Figure 1 shows the column density distribution along the  $y$ -direction for four different spatial scales at  $t = 6.90 \times 10^5$  yr, or  $t_p = 1.760 \times 10^4$  yr, where  $t_p$  denotes an elapsed time after the first sink particle formation. Figure 1(a) shows the whole computational domain. The filamentary cloud fragments into the several cloud cores, one of which forms stars. The filamentary cloud is disturbed by the turbulence, which was imposed on the initial condition. Figure 1(b) shows the

cloud core. The cloud core has a sharply peaked density distribution in agreement with molecular line observations toward MC27/L1521F (Onishi et al. 1999). The sink particles are associated with the peak position. The cloud core has a three-dimensional prolated shape and it exhibits smooth iso-density surfaces, in agreement with Matsumoto & Hanawa (2011).

On a smaller scale as shown in Figure 1(c), a triple system of sink particles can be seen. The sink particles are associated with several spiral arms, which correspond to the arc structures on a 1000 AU scale. The spiral arms are caused by the gravitational interaction between the sink particles and the envelope gas. The gas is accelerated by the gravitational torque from the orbiting sink particles, and the gas has a supersonic velocity of typically  $\sim 0.5$  km s<sup>-1</sup>, exciting shock waves of arc-shapes. Figure 2 shows the distribution of the line-of-sight velocity, which was evaluated as a first moment of velocity,  $\int v_y(\mathbf{r})\rho(\mathbf{r})dy / \int \rho(\mathbf{r})dy$ , assuming that the gas is optically thin. This figure is comparable to Figure 4 from Tokuda et al. (2014). The arc shape and the velocity range are in agreement with the observations of Tokuda et al. (2014).

Note that the disk-like structure on a 1000 AU scale, which is shown as a region with  $\log N [\text{cm}^{-2}] \gtrsim 23.5$  in Figure 1(c), is an infalling envelope. Its structure is not supported by rotation, and the rotation velocity is comparable to the infall velocity there. The  $Q$ -value of Toomre (1964) is larger than unity, indicating that the infalling envelope as well as the arcs are not significantly self-gravitating.

Figure 1(d) is a close-up view of the triple system. The sink particles are labeled by identification numbers 0, 1 and 2 in order of formation epoch (hereafter referred to as Sinks 0, 1, and 2). Sinks 0 and 2 constitute a close binary with a separation of 20 – 30 AU, while Sink 1 orbits around the close binary with a long separation of 100 – 200 AU. At the stage as shown in Figure 1, Sinks 0, 1, and 2 have masses of  $0.20 M_\odot$ ,  $0.32 M_\odot$ , and  $0.13 M_\odot$ , respectively. Sink 1 has the largest mass among the sink particles, and it has the largest circumstellar disk with a radius of  $\sim 30$  AU, while the other sink particles have small circumstellar disks with radii of  $\sim 7$  AU. The circumstellar disk of Sink 1 is relatively massive; the mass ratio between the disk and the sink particle remains at  $M_{\text{disk}}/M_{\text{star}} \sim 0.2$  for a long period of  $t_p \gtrsim 700$  yr, while other sink particles take ratios of  $M_{\text{disk}}/M_{\text{star}} \sim 0.003$ – $0.01$ . The massive disk of Sink 1 has the spiral arms caused by the gravitational instability; the disk exhibits the  $Q$ -value less than unity. They promote a high accretion rate onto Sink 1,  $\sim 2 \times 10^{-5} M_\odot \text{yr}^{-1}$ .

The circumstellar disk of Sink 2 is inclined with respect to the other circumstellar disks. The misalignment of the circumstellar disk is caused by tidal interactions from Sink 0 when Sink 2 undergoes successive close encounters with Sink 0 (c.f., Heller 1993). These close encounters are caused by the highly eccentric orbit of the tight binary pair of Sinks 0 and 2. During the evolution, rapid changes in the disk orientation occur several times for the disks of Sinks 0 and 2.

Figure 3 shows the changes in separation between all of the pairs of sink particles. In the early stages, four sink particles were formed and they exhibit chaotic orbits (Figure 3(b)). In their chaotic orbital motion, Sinks 1 and 3 merge at  $t_p = 3800$  yr (the cyan line). Subsequently, Sinks 1 and 2 form a close binary with a separation of 10 – 40 AU

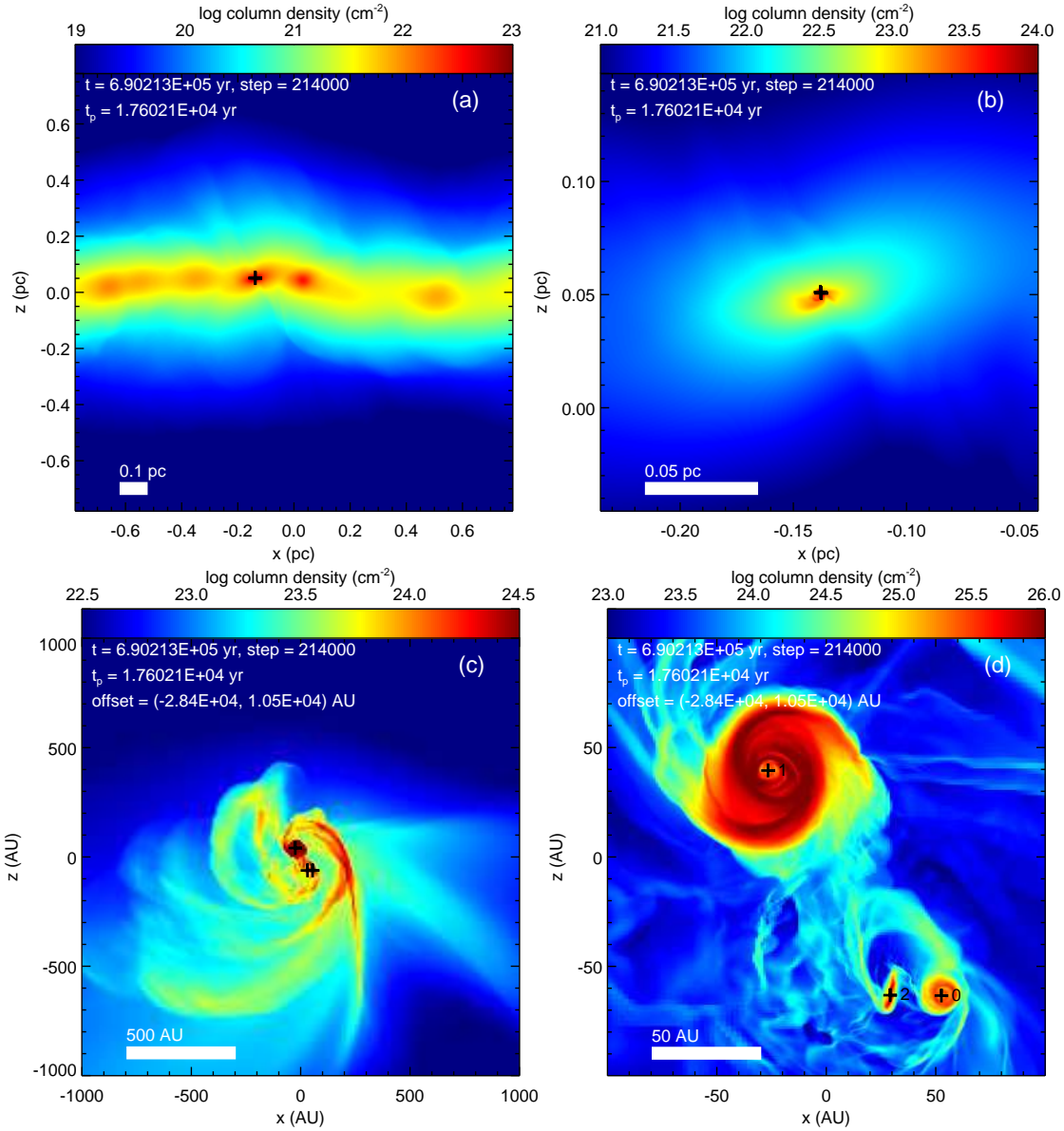


**Figure 1.** Column density distribution along the  $y$ -direction on four different spatial scales at  $t = 0.690$  Myr ( $t_p = 1.760 \times 10^4$  yr). The color scales depict the column densities. The black crosses indicate the positions of the sink particles. In panels (c) and (d), the coordinates are offset so that the center of each panel coincides with the center of mass of the sink particles. The sink particles are labeled with identification numbers 0, 1, and 2 in panel (d).

(the blue line). At  $t_p = 6000$  yr, Sink 0 approached the close binary of Sinks 1 and 2. Sink 0 and 1 were then exchanged to form a new close binary with Sinks 0 and 2. The orbit of Sink 1 then gradually decreases the eccentricity from 0.3 to 0.2 (the blue and red lines in Figure 3(a)). The close binary of Sinks 0 and 2 has a high eccentricity (the green line), leading to the misaligned circumstellar disks.

Because the sink particles have a chaotic epoch after their formation, the density structure in the infalling envelope, such as the arc, depends on the realization of the initial turbulence. We simulated the same model as the previous one but changed the random seed when generating the turbulence. Figure 4 shows the column density distribution at  $t = 8.15 \times 10^5$  yr ( $t_p = 2.14 \times 10^4$  yr). By this

stage, this realization model has produced six sink particles in total and they eventually merge into three sink particles. The sink particles undergo chaotic orbital motions until  $t_p \simeq 2 \times 10^4$  yr, which is a considerably longer period than in the previous model. This realization model also exhibits arc structures on a 1000 AU scale. The line-of-sight velocities of the arc structures also range within  $\sim \pm 0.5 \text{ km s}^{-1}$ . This model also exhibits misaligned circumstellar disks caused by close encounters between sink particles. In the stage shown in Figure 4, the most distant sink particle (Sink 0) has a circumstellar disk inclined with respect to the other circumstellar disks.

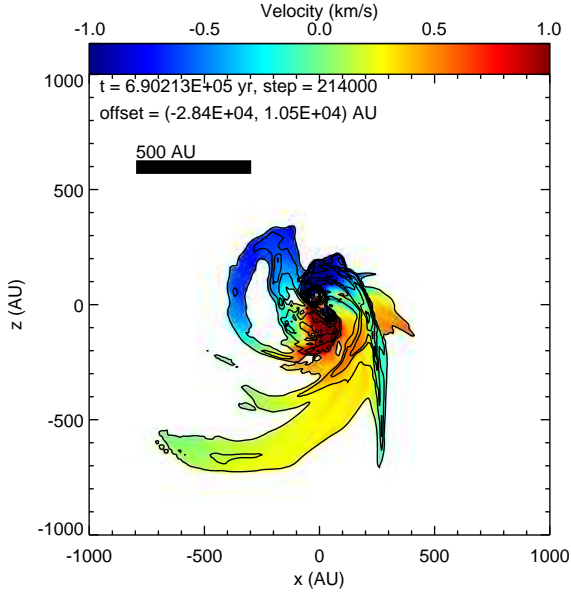


**Figure 2.** Line-of-sight velocity distribution in the arc structures. The color scale shows the velocity along the line of sight. The contour shows the column density on a logarithmic scale with  $\log(N/\text{cm}^{-2}) = 23.4, 23.6, \dots$ , where  $N$  denotes the column density. The velocity is shown only in the regions where the column density is greater than the lowest contour level.

#### 4 SUMMARY AND DISCUSSION

We demonstrated the formation of arc structure on a 1000 AU scale in the infalling envelope during the early phase of star formation as a consequence of the collapse of a weakly turbulent cloud core. The density and velocity structures reproduced here are in agreement with the arc structure revealed by the recent ALMA observations toward MC27/L1521F. We also found that the misaligned disks are formed in triple systems.

According to Tokuda et al. (2014), MC27/L1521F has three high-density condensations observed by the dust continuum, one of which (MMS-1) was also observed by the Spitzer space telescope (Bourke et al. 2006). The other two condensations (MMS-2 and MMS-3) have high densities of  $10^{6-7} \text{ cm}^{-3}$ , and MMS-2 is a candidate for the first core as predicted by Larson (1969).

A possible interpretation for these high-density condensations is that they are formed by fragmentation during the protostellar collapse of the cloud core as shown in our simulations. The velocity of the arc structure is ranged typically within  $\sim \pm 0.5 \text{ km s}^{-1}$ , and it is consistent with the dynamical velocity of the system, e.g., the Kepler velocity for a mass of  $0.2 M_{\odot}$  and a radius of 500 AU. Moreover, the time scale of the arc structure is  $1000 \text{ AU}/0.5 \text{ km s}^{-1} \simeq 10^4 \text{ yr}$ , in agreement with the epoch shown in Figure 1,  $t_p = 1.760 \times 10^4 \text{ yr}$ . However, a few issues remain unsolved in the following points. First, the masses of the sink particles grow exceeding  $0.1 M_{\odot}$  with this time scale. These masses are greater than those reported by Tokuda et al. (2014). Second, MMS-2, the first core candidate, may have a short lifetime of less than 1000 yr according to the recent radiation-transfer MHD simulations by Tomida et al. (2013). Within such a short pe-

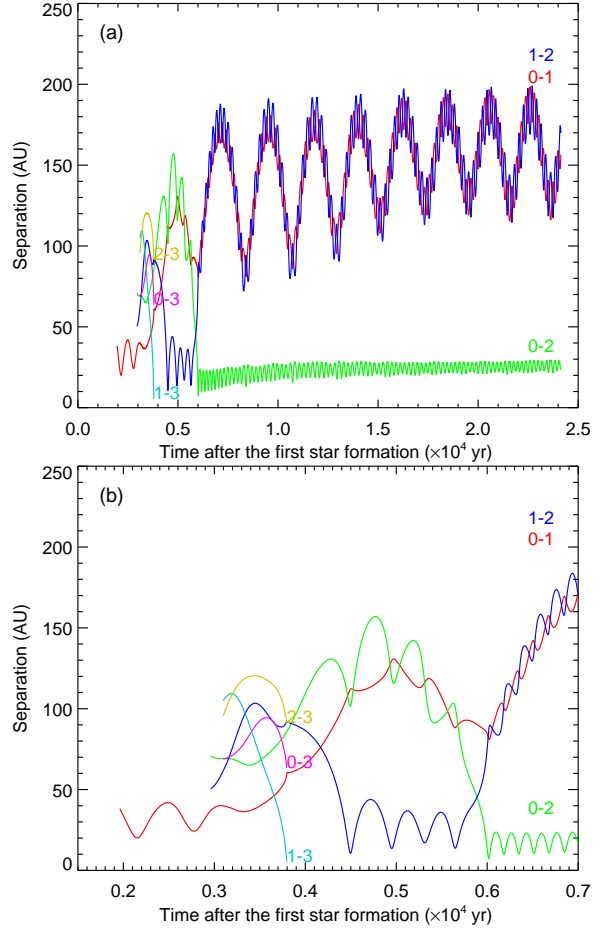


**Figure 3.** Separations between all of the pairs of sink particles as a function of time after the first sink particle formation. The label  $n - m$  associated with each line indicates the separation between Sinks  $n$  and  $m$ . Panel (b) is an enlargement of the chaotic period in the early phase.

riod, an arc structure can not extend to a 1000 AU scale with its typical velocity of  $\sim 0.5 \text{ km s}^{-1}$ .

Protostars undergo chaotic orbits in the period of several  $\times 10^3 - 10^4 \text{ yr}$  after their formation. Their chaotic orbits influence the evolution of multiple stars as well as the surrounding envelope, such as the arc structures. The gravitational few-body problem is therefore a key issue in the early phase of low-mass star formation. This is somewhat analogous to the interactions in “the competitive accretion scenario” for massive star formation (Bonnell et al. 2004), in which the gravitational N-body problem is supposed to govern the dynamics of clusters and therefore accretion.

Another scenario to consider for the formation of an arc structure is a magnetic wall around the protostars. The formation of a magnetic wall was predicted by some theoretical works (e.g., Li & McKee 1996; Tassis & Mouschovias 2005; Zhao et al. 2011). The three-dimensional simulations showed that the magnetic wall produces cavities in the infalling envelope. The rims of the cavities have higher densities than the envelope and they may be observed as arc structures. However, the magnetic field suppresses fragmentation for the typical parameters of molecular cloud cores (Machida et al. 2005). The formation mechanism of the



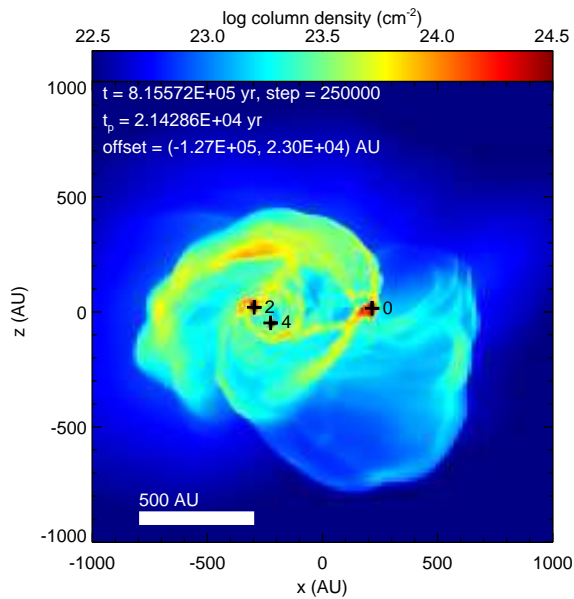


**Figure 4.** Column density distribution showing arc structures. The black crosses indicate the positions of the sink particles, which are labeled with identification numbers. The realization is different from that shown in Figure 1.

high-density condensations, MMS-2 and MMS-3, can then not be explained by the fragmentation process. The observed arc structure therefore implies that the magnetic field is weak enough to promote fragmentation of the cloud core.

Misalignment of a circumstellar disk is caused by the tidal interaction with sink particles when they undergo close encounters. The close encounters are promoted by the chaotic orbits in a triple system. Thus, triple systems are expected to have misaligned circumstellar disks, and to also be associated with arc structures if they are young enough to be embedded in the dense envelope.

Misaligned disks were reported for the young binary system, HK Tau (Jensen & Akeson 2014), AS 205 (Salyk et al. 2014), and V2434Ori (Williams et al. 2014) based on the recent ALMA observations. The young triple system, T Tau, includes the tight binary of T Tau Sa and T Tau Sb, and the existence of a misaligned circumstellar disk has been indicated therein (Skemer et al. 2008; Ratzka et al. 2009). Our model suggests that this misaligned disk could be caused by the tidal interaction between the tight binary pair in the triple system.

## ACKNOWLEDGMENTS

Numerical computations were carried out on Cray XC30 at the Center for Computational Astrophysics, National Astronomical Observatory of Japan. This research was supported by JSPS KAKENHI Grant Numbers 26400233, 26287030, 24244017, 23540270, 23403001, 23244027, 23103005, 22244014.

## REFERENCES

- André, P., Men'shchikov, A., Bontemps, S., et al. 2010, *A&A*, 518, L102
- Arzoumanian, D., André, P., Didelon, P., et al. 2011, *A&A*, 529, L6
- Bate, M. R., Bonnell, I. A., & Bromm, V. 2002, *MNRAS*, 332, L65
- Bonnell, I. A., Vine, S. G., & Bate, M. R. 2004, *MNRAS*, 349, 735
- Bourke, T. L., Myers, P. C., Evans, N. J., II, et al. 2006, *ApJ*, 649, L37
- Codella, C., Welser, R., Henkel, C., Benson, P. J., & Myers, P. C. 1997, *A&A*, 324, 203
- Dubinski, J., Narayan, R., & Phillips, T. G. 1995, *ApJ*, 448, 226
- Goodwin, S. P., Whitworth, A. P., & Ward-Thompson, D. 2004, *A&A*, 414, 633
- Hacar, A., Tafalla, M., Kauffmann, J., & Kovács, A. 2013, *A&A*, 554, A55
- Heller, C. H. 1993, *ApJ*, 408, 337
- Jensen, E. L. N., & Akeson, R. 2014, *Nature*, 511, 567
- Larson, R. B. 1969, *MNRAS*, 145, 271
- Larson, R. B. 1981, *MNRAS*, 194, 809
- Li, Z.-Y., & McKee, C. F. 1996, *ApJ*, 464, 373
- Machida, M. N., Matsumoto, T., Hanawa, T., & Tomisaka, K. 2005, *MNRAS*, 362, 382
- Masunaga, H., Miyama, S. M., & Inutsuka, S. 1998, *ApJ*, 495, 346.
- Matsumoto, T., & Hanawa, T. 2011, *ApJ*, 728, 47
- Matsumoto, T., Dobashi, K., & Shimoikura, T., 2015, *ApJ*, 801, 77
- Matsumoto, T. 2007, *PASJ*, 59, 905
- Mizuno, A., Onishi, T., Hayashi, M., et al. 1994, *Nature*, 368, 719
- Nagasawa, M. 1987, *Progress of Theoretical Physics*, 77, 635
- Onishi, T., Mizuno, A., Kawamura, A., Ogawa, H., & Fukui, Y. 1998, *ApJ*, 502, 296
- Onishi, T., Mizuno, A., & Fukui, Y. 1999, *PASJ*, 51, 257
- Onishi, T., Mizuno, A., Kawamura, A., Tachihara, K., & Fukui, Y. 2002, *ApJ*, 575, 950
- Ostriker, J. 1964, *ApJ*, 140, 1056
- Ratzka, T., Schegerer, A. A., Leinert, C., et al. 2009, *A&A*, 502, 623
- Salyk, C., Pontoppidan, K., Corder, S., et al. 2014, *ApJ*, 792, 68
- Skemer, A. J., Close, L. M., Hinz, P. M., et al. 2008, *ApJ*, 676, 1082
- Stodólkiewicz, J. S. 1963, *Acta Astron.*, 13, 30
- Tassis, K., & Mouschovias, T. C. 2005, *ApJ*, 618, 783
- Tokuda, K., Onishi, T., Saigo, K., et al. 2014, *ApJ*, 789, L4
- Tomida, K., Tomisaka, K., Matsumoto, T., et al. 2013, *ApJ*, 763, 6
- Toomre, A. 1964, *ApJ*, 139, 1217
- Truelove, J. K., Klein, R. I., McKee, C. F., Holliman, J. H., II, Howell, L. H., & Greenough, J. A. 1997, *ApJ*, 489, L179
- Williams, J. P., Mann, R. K., Di Francesco, J., et al. 2014, *ApJ*, 796, 120
- Zhao, B., Li, Z.-Y., Nakamura, F., Krasnopolsky, R., & Shang, H. 2011, *ApJ*, 742, 10